Performance of laterally elongated pillar array columns in capillary electrochromatography mode

Baca, Martyna; Kryj, Agata; Naghdi, Elahe; Gelin, Pierre; Sukas, Sertan; Laha, Priya; Terryn, Herman; Ottevaere, Heidi; De Malsche, Wim

Published in:
Electrophoresis

DOI:
10.1002/elps.202000001

Publication date:
2020

Document Version:
Accepted author manuscript

Performance of laterally elongated pillar array columns in capillary electrochromatography mode

Martyna Baca[1], Agata Kryj[1], Elahe Naghdi[2], Pierre Gelin[1], Sertan Sukas[1], Priya Laha[3], Herman Terryn[3], Heidi Ottevaere[4], Wim De Malsche[1*]

[1]µFlow group, Department of Chemical Engineering, Vrije Universiteit Brussel Brussels B-1050, Belgium

[2]Faculty of Chemistry, Shahid Beheshti University, G.C., Tehran, Iran

[3]Research Group Electrochemical and Surface Engineering (SURF), Vrije Universiteit Brussel, Brussels B-1050, Belgium

[4]Department of Applied Physics and Photonics, Vrije Universiteit Brussel, Brussels B-1050, Belgium

(*) corresponding author

Pleinlaan 2, B-1050, Brussels, Belgium

Abstract

In the present study, cylindrical and laterally elongated pillar array columns were investigated for use in capillary electrochromatography. Minimal theoretical plate heights of H=1.90 µm and H=1.46 µm (in absence of sidewall effect) were obtained for coumarin C440 under unretained conditions for cylindrical and rectangular (laterally elongated, aspect ratio 4) pillar array columns, respectively. By comparing dispersion at the entire channel width to that at the central zone only, it appears that sidewall related dispersion significantly contributes to overall dispersion. A 40 % reduction of the plate height was observed by taking into account only the central channel zone.

A kinetic plot analysis was performed to evaluate the potential of the studied geometries by considering a maximum operating voltage of 20 kV as limiting parameter. It was demonstrated that rectangular radially elongated pillars produce a higher efficiency than cylindrical pillars and other microfabricated column structures for microchip capillary electrochromatography previously studied.

1. Introduction

Capillary electrochromatography (CEC) in open-tubular columns and microfluidic chips is an attractive alternative to capillary electrophoresis (CE) and high-performance liquid chromatography (HPLC), techniques that utilize the principles of electrophoresis and chromatography [1, 2, 3], respectively. The origin of CEC can be traced back to 1974 when Pretorius proposed the use of electroosmotic flow to transport the mobile phase through the column and reported that in comparison to the hydrodynamic flow, the plate height was reduced [4]. Important landmark contributions are also the work of Jorgenson and Luckas [5], who demonstrated the first CEC separation of non-ionic compounds in a packed capillary column.

More fundamental aspects and advantages of CEC have been extensively studied by, among others, Knox and Grant [6,7,8]. In CEC, the flow of the mobile phase is driven through the column by means of an electroosmotic flow (EOF), which is generated by axially applying a high voltage across the column. An electroosmotic flow generates a flat flow profile that reduces band dispersion and therefore narrower peaks, a better resolution and higher efficiencies can be achieved in comparison with conventional pressure-driven HPLC [9]. A higher plate count (N) and smaller theoretical plate heights (H) result from reduced contributions to H from reduced eddy diffusion (A-term) and reduced resistance to mass transfer in the mobile and stationary phase (C-term) [10, 11]. A factor that can reduce the column efficiency in CEC column is Joule heating [12]. Knox and Grant reported that a reduction of column diameter can prevent temperature gradients [6], which stimulates the use of miniaturized column formats for CEC operation. A wide variety of column lengths and particle sizes have already been used for CEC, yielding high plate counts [13]. For instance, Dadoo *et al.* demonstrated 750,000 theoretical plates/m detected prior to the outlet frit in a 30 cm packed bed containing 1.5 μm non-porous particles in a 100 μm i.d. fused silica capillary [14]. Ludtke *et al.* reported efficiencies of up to 288,800 plates per meter for a test solute of n-alkylbenzenes on an 8.6 cm packed bed of 0.5 μm C8 particles [15]. Smith and Evans obtained 387,000 plates/m for a retained pharmaceutical compound (k = 4.3) on 50-μm capillaries packed with 3-μm porous ODS-1 particles [16]. Efficiency results in CEC however need to be interpreted with care, as often surprisingly high efficiency can be attributed to electrostatic peak focusing phenomena [21-24], and therefore does not always reflect plate height values but predominantly band focusing. More modest plate counts were reported by Lynen et al., yielding a plate height of 6.31 μm for octanophenone using a packed column with 3-μm Hypersil-C18 particles (335 mm × 100 μm i.d.) for CEC separations. Based on the kinetic plots, the authors predicted that for octanophenone 120,000 plates over a length of 1.5 m will be

obtained. Moreover, they observed a significant increase in CEC column performance operated at lower temperature (10 °C), indicating better control of the Joule heating phenomenon. Also, kinetic plot extrapolations were performed towards the use of smaller particles (0.5 μm) and higher voltages (120 kV), wherein 820,000 plates are predicted to be achievable (k'=1.67) in 144 min [24]. The ability to apply a potential as high as 300 kV has been already demonstrated by Jorgenson group for ultra-high voltage capillary electrophoresis (UHVCE). They separated a sample of 3 peptides and 3 proteins using a 900 cm coated capillary at −263 kV, producing over 2 million theoretical plates for peptides [25]. Other column formats such as open-tubular, monolithic and pillar array columns have been so far explored as an alternative to packed columns.

Microfluidic chips possess several attractive advantages compared to traditional columns, such as smaller physical dimensions that can reduce the reagent consumption or efficient heat transfer for lower dispersion [26]. The first electrochromatography separation on a microchip was presented by Jacobson et al. in 1994 and involved functionalization of the surface of an open channel glass microchip with octadecylsilane (C18) for a reversed phase separation of neutral analytes [27]. Later, Ramsey and coworkers demonstrated separations on a glass microchip with a 16.5 cm long serpentine channel that was 5.6 μm deep and 66 μm wide [28]. In 1998, Regnier and co-workers presented an alternative so-called collocated monolithic support structure format, composed of a structured array of pillars [29]. The Regnier group studied the impact of different pillar geometries, including channel depths of 1.6−10 μm, pillar distances of 2−4 μm, and several pillar shapes including diamonds with sides of 5−11 μm, and their elongated and extended versions in CEC separations [29] using PDMS as support structures. Due to the poor definition quality of the pillars related to the used PDMS casting process (non-vertical pillars that are rounded at the top region), interconnectivity was critical to account for defects in the support structures. As a result, in contrast to what can be expected

for an ideal and perfectly defined pillar array column, elongation resulted in a reduction of performance. The Regnier group also developed quartz devices with much better definition control than PDMS, with pillar dimensions of 1.5 x 10 μm [30] in a tilted rectangular shape, demonstrating 35,000 plates in a 4.4 cm channel (plate height H=1.3 μm).

Sukas et al. studied the chromatographic performance of additional designs for microfabricated column structures for microchip capillary electrochromatography with as a goal to simultaneously optimize electroosmotic mobility and plate height. Minimum plate heights of 0.77, 1.33, and 1.42 μm for foil, diamond, and hexagon were obtained, respectively, when applying an electric field of 1 kV/cm under unretained conditions. In retained mode, minimum plate height values of 1.85 and 3.28 μm for foil and diamond, respectively [31], were obtained.

Silicon-based pillar array columns (PACs) have been studied intensively by our and other groups in pressure driven-mode [32-37], originally for their low or even absent A-term contribution in dispersion. It has been demonstrated that radially elongated pillars (REP) can reach the same separation impedance (proportional to the time required for a given separation at a given pressure drop) as open tubular columns, but with channel widths of 1000 μm for the REPs compared to the 2.5 μm value for the OTCs, showing therewith greatly increased loadability of the column and, as a consequence, also detection sensitivity [38]. Whereas radial elongation was originally implemented to reduce sidewall effects, an important finding was that REPs also led to a large reduction of B-term dispersion [39]. Sidewall related dispersion occurs in pillar array columns because of a (repeated and therefore often considerable) velocity mismatch of the mobile phase (and sample components) between the central part of the channel and the wall. To assess this effect the band variance of the central region only is used to calculate the dispersion of the central region (hence excluding sidewall related dispersion). Callewaert *et al.* reported the reduction of the minimum plate height from 0.42 μm to 0.25 μm

for non-retained conditions and from 0.77 μm to 0.57 μm for retained conditions (k=1.0), when going from AR=12 to AR=20 (AR is the height-to-width ratio of etched features) [39].

The aim of the present study is to exploit the B-term reduction feature of radially elongated structures for electrically instead of pressure driven systems, as well as to study the impact of the shape on other performance parameters as sidewall dispersion and electroosmotic mobility. The use of laterally elongated pillars has been studied before using PDMS devices, but did not offer a performance gain due to the fact that PDMS has too many imperfections and that the lower interconnectivity that (axially or radially) elongated structures bring about, result in a loss of performance [29]. The main research question of the present study is whether radial elongation using columns patterned with glass structures by deep reactive ion etching, where the need for interconnectivity to reduce the impact of imperfections is less stringent, can improve the performance of CEC. To this end, we evaluate arrays of cylindrical (aspect ratio AR=1) and rectangular (AR=4) pillars.

2. Materials and methods.

2.1. Chemicals and materials

Sodium dihydrogen phosphate (≥99.0%), disodium hydrogen phosphate (≥99.0%), sodium hydroxide (HPLC grade, 50.0%) were purchased from Sigma-Aldrich (Diegem, Belgium). Methanol (LC–MS grade) obtained from Bio-solve B.V. (Valkenswaard, NL). Coumarin 440 (C440: 7-amino-4-methyl-2H-1-benzopyran-2-one) were purchased from Sigma-Aldrich (Diegem, Belgium), (C480: 2,3,6,7-tetrahydro-9-methyl-1H,5H,11H-[1]benzopyrano-[6,7,8-ij]quinolizin-11-one) were purchased from Vadeno Optical Solutions (Apeldoorn, NL). Deionized HPLC-grade water was produced in-house using a Milli-Q water purification system (Millipore, Molsheim, France).

145 Pillar array glass columns were fabricated at the University of Twente (Enschede,
146 Netherlands). The chips contain channels with a length of 2 cm and a width of 500 µm. The
147 first design contains cylindrical pillars (5 µm diameter, 5 µm deep, 5 µm interpillar distance).
148 The second design contains rectangular pillars (5 µm × 20 µm pillar size, 5 µm deep, 5 µm
149 interpillar distance). The process is identical as described in Sukas *et al.* [31].

150 The devices were patterned using a 2-mask process. First, a 1 µm thick poly-silicon (poly-Si)
151 layer was deposited via LPCVD (Tempress Systems) on a 100 mm diameter fused silica wafer
152 with 500 µm thickness (Schott Lithotech) right after cleaning in liquid and fuming nitric acid
153 solutions. A 1.2 µm thick photoresist (Olin 907-12) layer was spin-coated at 4000 rpm
154 followed by UV-photolithography for transferring the channel layout. As a next step, the poly-
155 Si layer was etched through by DRIE (Adixen AMS100SE). Afterwards, the patterned poly-
156 Si layer was used as a hard mask for etching fused silica by another DRIE step (Adixen
157 AMS100DE). Subsequently, a thick photoresist film (Ordyl BF410) was laminated on the
158 backside of the wafer and patterned with UV-photolithography. The film served as a mask for
159 through etching of the wafer to open the access holes for the fluidic connections, via powder
160 blasting (with 29 µm alumina particles), using an in-house built setup. After powder blasting,
161 the wafer was first washed with DI-water and then immersed in acetone and isopropanol,
162 respectively. The poly-Si layer was etched away in KOH solution after a cleaning cycle in
163 nitric acid. Next, a bare fused silica wafer was cleaned with the same procedure and directly
164 bonded with the processed wafer in order to obtain closed channels. Then, the bonded stack
165 was kept in a high temperature furnace for the permanent bond for 36 hours with ramping up
166 to a maximum temperature of 1080 °C and cooling down back to room temperature with
167 specified rates. As a final step, the stack was diced, and individual microchips were fabricated
168 successfully.

169 2.2 Instrumentation

An 8-channel high voltage power supply (Labsmith HVS448-6000D, Mengel Engineering, Virum, Denmark) was used to apply a voltage across the channel and to perform the CEC measurements. Fluorescence microscope setup was used to perform on-chip detection. The microscope consisted of an inverted microscope IX-71 equipped with the U-RFT-T lamp power supply (Olympus, Tokyo, JP), an electron multiplier CCD camera C9100-13 (Hamamatsu Photonics, Shizuoka, JP), a XF1075387AF28 (wavelength, 360–420 nm; Omega Optical Inc., VT, USA) for the excitation filter, and a MF460-80 (wavelength, 400−500 nm; Thorlabs Elliptec GmbH, Dortmund, DE) for the emission filter. The whole detection set-up, together with a linear displacement stage (M-TS100DC) and a speed controller (MM, 400 Newport), is mounted on a breadboard (M-IG 23-2, Newport, The Netherlands). A home-built pressure vessel system was used to flush channel of the microchips before and after conducting the experiments.

2.3. Mobile-phase and sample preparation.

25 mM buffer phosphate with 50% methanol (MeOH) was used as mobile phase. Buffer phosphate was prepared by dissolving the desired concentration of sodium dihydrogen phosphate, and disodium hydrogen phosphate to obtain 0.05 mM concentration. The pH of the mobile phase was adjusted to a value of pH = 7.0 by the addition of 50% sodium hydroxide solution. The final mobile phase solution was prepared by diluting 50 mM sodium phosphate with pure MeOH, resulting in a 25 mM buffer phosphate with 50% MeOH. Coumarin dyes (C440, C480) were first dissolved in HPLC-grade methanol to obtain the stock solution of 10 mM and then they were diluted with 50/50 methanol/buffer phosphate pH 7 to obtain a final concentration of 5 mM. Prior to use, mobile phases and samples were always filtered over 0.2 μm PTFE filter (Pall Corporation, HPLC Certified, Puerto Rico).

2.3. Chip coating procedure.

Firstly, the chip was flushed with methanol, followed by 50% methanol/toluene (v/v), and then toluene (12 h each) by applying nitrogen gas pressure of 20 bar on the to be pumped liquid. C18-modification was carried out with a continuous flow of a 10% octadecyldimethyl-N,N-diethylaminosilane solution in toluene (ODS-DMA)/toluene (v/v) under 30 bar (overnight) at 60 °C. Amino group is the most reactive and provide the best bonding among other reagents containing halogen atoms like *e.g:* Cl, Br, I. Afterwards, the chip was consecutively flushed with toluene, 50% methanol/toluene (v/v), and methanol for 12 h each.

2.4 Experimental procedure.

The chips were placed in a home-made CNC-machined plastic (Delrin, acetal homopolymer) holder consisting of a bottom-plate with a window to observe the microchannel, and a top-plate with four drilled through holes compatible with commercially available Nanoport® connectors (Achrom, Belgium), that allow to have around 200 µL mobile phase and sample reservoirs. Before starting experiments, the entire chip surface was wetted and possible impurities from previous measurement were removed by flushing the chip with methanol for 20 min at 20 bar. After that, buffer phosphate (pH 7, 50 mM concentration) mixed with 50:50 MeOH volumetric composition was pumped with a pressure of 20 bar for 20 min. Before starting the experiment, all reservoirs were filled with the solution of buffer phosphate 50 mM/ methanol 50/50 (v/v) and a 5 mM C440 solution was dispensed into the sample inlet reservoir. Afterwards, platinum wires, which serve as the electrodes, were immersed inside the reservoirs and the voltages were applied. Injection was performed by applying 400 V/cm electric field through the injection channel with pinching. Subsequently, the accumulated sample at the injection cross was pushed into the separation channel by applying electric fields varying from 0.3 to 2.1 kV/cm (Fig. 1).

2.5 Detection & data processing.

On-chip fluorescence spectroscopy was used as detection method. The peaks were monitored at 2 mm translation distance downstream the injection zone. The fluorescence microscope images, and movie files were processed with an in-house written script in MatlabR2018a software (Mathworks, MA, USA) to obtain chromatographic data. For the determination of the peak widths and plate heights, the fluorescence intensity was averaged across the channel width. Further, obtained axial concentration distribution was fitted using the Matlab Gaussian fitting algorithm ($y = ae^{-(\frac{x-b}{c})^2}$). The initial band was observed at the start of the channel (on-chip). The plate height values were obtained as $(\sigma_{x.e}^2 - \sigma_{x,0}^2)/\Delta x$, wherein $\sigma_{x,e}$ and $\sigma_{x,0}$ are the peak variance of the injected band at the end and the initial position and Δx is the distance between the two positions.

3. Results and discussion

Fig. 2 shows optical images of the studied cylindrical and rectangular pillar array columns, both having an interpillar distance of 5 μm. Fig. 3 shows cross-section SEM (Scanning Electron Microscopy) images. As can be seen the pillars are slightly tapered, which is a consequence of the plasma etching process of the fused silica substrate. This is in contrast with typical Bosch etching processes dedicated to silicon, for which near to 90 ° angles are typically observed [40, 41]. For the studied fused silica device, the spacing of the pillars is 5.5 μm at the central and top part of the pillar, whereas it is about 6.5 μm at the bottom (see Fig. 3a). In Fig. 3b, also tapering of the structures can be observed (albeit less pronounced). Significant deviations in top and bottom dimensions can be observed at the sidewall region of both designs.

Next, flow experiments were performed. Fig. 4 shows the injected initial and final band together with corresponding peak profiles measured 2 mm downstream from the injection zone

242 at 476 V/cm on a cylindrical pillar array column. Fig. 5 shows a chromatogram obtained for
243 two coumarin dyes (C440, C480) with a C18-modified cylindrical pillar array column (see
244 experimental section for details). 40% methanol/buffer phosphate, pH=7 (v/v) was applied as
245 mobile phase and fluorescence detection was conducted at 4 mm downstream the injection
246 zone. The separation of coumarin C440 and C480 was achieved in 30 seconds with a resolution
247 of 1.30. To evaluate the performance of the columns, unretained van Deemter plots were
248 established (Fig. 6). Minimal plate heights for C440 (unretained conditions) of H= 3.16 µm
249 were obtained for cylinders, and H= 2.40 µm for rectangles (aspect ratio AR=4). By excluding
250 side wall regions and taking into account only the central part (400 µm wide zone) of the
251 channel, further reduction of the minimal plate heights to 1.90 µm for cylinders and 1.43 µm
252 for rectangles were observed. The difference in plate height values is related to the fact that,
253 due to the inevitable difference in local flow conditions and available surface at the central
254 region and at the sidewall region are different. A similar observation has been made with
255 pressure driven operation as well, where dramatic sidewall induced band broadening occurs,
256 even when the target dimension is off-target [36, 42]. In pressure-driven work, it was
257 demonstrated that at increasing lateral elongation of pillars, a much lower sensitivity was
258 detected to sidewall dispersion [43]. In fig. 6, a similar increase is observed for both AR=1
259 (cylindrical) and AR=4 (rectangular).

260 The optimal linear velocities for cylindrical pillar array column were 0.38 mm/s,
261 corresponding to an electric field of 540 V/cm and for rectangles were 0.19 mm/s
262 corresponding to the electric field of 477 V/cm. A reduction in H_{min} with increasing AR is in
263 line with theoretical expectations [44], as axial diffusion is reduced due to increased obstruction
264 for diffusion in the axial direction at increasing AR. This is reflected in a reduced B-term at
265 increasing AR (see table 1). The C-term is however considerably larger for the rectangular
266 pillar design. This is thought to be mainly related to the considerable taper near the sidewall

region that can be observed in Fig. 2The C-term originating from the pillar bed located remote from the sidewall is lower for rectangles (see table 2), indicating that the rectangular shape is more advantageous for C-term dispersion In table 2, also the values of earlier studies wherein the pillars are shown (in grey).

Table 1: A, B and C terms of the fitted van Deemter curves for the studied design including sidewall effect.

	Cylinders	**Rectangles**
A (mm)	5.5E-4	2.2E-4
B (mm^2/s)	5.3E-4	2.7E-4
C (s)	4.3E-4	5.67E-3

Table 2: A, B and C terms of the fitted van Deemter curves for the studied design without the sidewall effect, and designs (foil 0°, foil 25°, hexagon and diamond) studied by [31].

	Cylinders	**Rectangles**	**foil 0°**	**foil 25°**	**hexagon**	**Diamond**
A (mm)	3.70E-4	9.1E-4	1.0 E-6	7.6E-4	8.0E-5	0
B (mm^2/s)	4.4E-4	1.2E-4	9.2E-4	1.0E-3	9.0E-4	1.0E-3
C (s)	2.2E-3	0	1.4E-4	2.2E-4	4.8E-4	4.1E-4

The A term in the van Deemter equation is relevant to the channel geometry of the microfluidic chip and the value in this study was on the order of 10^{-4} mm which is related to the uniform packing and structure definition of the column. Rectangular structures yielded the lowest B-term, related to the increasing obstruction of diffusion at increasing AR. In the context of pressure driven separation, it has been demonstrated that plate heights could drop over 80% by increasing the pillar aspect ratio from 1.2 to 15, mainly due to a 25-fold reduction in the measured B-term [38]. In the present study wherein, the flow has an electroosmotic origin, the lowest plate height value of 1.43 μm (in the absence of sidewall effects) was achieved for rectangles. This is slightly higher than the plate height values obtained by Sukas *et al.* [31], who obtained a value of 0.77 μm for the 0° foil shape and 1.42 μm for the hexagon shape. Because the plate height scales with the characteristic dimensions of the system, it should be

stressed that an important difference between our study and that of Sukas *et al*. [31] is that the spacing of the pillars is 5 µm and about 2 µm, respectively. As spacing between the pillars decreases, lower plate heights are expected.

Based on the geometrical improvement observed here, it is possible to gain performance by further scaling down the system. For CEC, the electroosmotic mobility can be obtained from Fig. 7 as a slope of linear flow velocity versus electric field strength. The obtained electroosmotic mobility of the cylindrical pillar array column was found to be 6.0×10^{-9} m^2/Vs, which is higher than that of rectangular pillar array column (4.0×10^{-9} m^2/Vs). As expected, the EOF velocity was higher in cylindrical pillar array columns than in rectangular, this is related to the fact that the path length increases with lateral elongation and that hence the effective field strength (locally oriented along the flow-through channels) is reduced.

For the electric field of 475 V/cm, the measured mobile phase velocities were 0.27, and 0.19 mm/s for cylinders and rectangles, respectively. A rectangular pillar shape with AR=4 had a 56% lower mobility when compared to a cylindrical pillar array column. The total analysis is however determined by both the electroosmotic permeability and the plate height, with a maximal electrical potential value as an additional (boundary) parameter. Above the 400 V/cm (1.2 kV), the EOF velocity is no longer a linear function of electric field. The reason of the non-linearity can be related to the Joule heating (causing current breakdown). Joule heating is caused by the power dissipation that leads to an increase in the temperature of the electrolyte, hence an increase in diffusion coefficient and mobility but also may create a temperature gradient over the channel. This results in a non-linearity in velocity–field strength relationship. It has been found that our measured values of the electroosmotic mobility are about an order of magnitude lower in comparison to data obtained by Sukas *et al*. [31]. This is related to differences in geometry and the fact that we have lateral elongation (see above). Also worth mentioning is the fact that the mobile phases of both studies did not have the same composition

313 (in [31] a pH value of 9 as used, whereas in the present study a value of pH=7 was used).We
314 have also included some characteristic values of electroosmotic permeabilities of packed bed
315 (see grey values in table 3).

316 **Table 3:** The comparison of measured values of the electroosmotic mobility for cylindrical and
317 rectangles pillar array columns with the data obtained by Sukas *et al.* for foil 0°, foil with 25°
318 tip angle, for hexagon, and for diamond [31]. The plate height values for 3.5 μm porous
319 particles and 2 μm nonporous particles were derived from the paper of Choudhary *et al.* [45].

	cylinders	**rectangles**	**foil 0°**	**foil 25°**	**hexagon**	**diamond**	**3.5 μm porous particles**	**2 μm non porous particles**
Electroosmotic mobility (m^2/Vs)	6.0E-9	4.0E-9	1.68E-8	1.60E-8	1.54E-8	1.44E-8	3.3E-8	4.6E-8

320

321 In CEC, the maximum efficiency of the column is just determined by the mobility of
322 the electro-osmotic flow (EOF). In comparison to the pressure driven mode, CEC kinetic plot
323 can be constructed by implementing the values of the efficiency and the potential drop. Linear
324 mobile phase velocity can be calculated as follows:

325 $$u_0 = u_{EOF}\frac{\Delta V}{L}$$

326 Kinetic plot in CEC can be described by the following equations:

327 $$N = u_{EOF}\frac{\Delta V}{H u_0}$$

328 $$t_0 = u_{EOF}\frac{\Delta V}{u_0^2}$$

329 where u_{EOF} represents the electro osmotic flow mobility, ΔV is an applied voltage and L is a
330 total length of the column [ref].

In the same manner as in case of pressure driven techniques [46], kinetic plots here are obtained by extrapolation to the maximum voltage [24, 31]. Fig. 8 compares the kinetic performance of the two analyzed structures (cylindrical and rectangular) in the non-retained mode for a 20 kV voltage drop. We have also included literature values of Sukas *et al.* for comparison (grey curves). For structures with an aspect ratio (axial/lateral elongation) below or equal to 1, a limit of around N= 2.5×10^5 plates are observed for cylindrical pillars wherein no sidewall effects is present. For the sidewall containing plots, the performance is, as expected, lower than for the plots wherein sidewall effects are excluded (only observing in the central part of the channel). The optimal kinetic value (maximal plates/unit time) for cylinders is achieved around 130 min, yielding 2.5×10^5 plates. Not unexpectedly, the cylindrical format has a lower performance than the optimized foil shaped pillars of Sukas *et al.* [31], where at the optimal value around 5.4×10^4 plates are generated with the attainable plates number limit set at around 3.7×10^5. For the rectangular (AR=4) channels, the B-term is further reduced, resulting in a higher performance. The plate counts of 4.5×10^5 can be obtained in 296 min using a column length of 1.19 m. The B-term reduction is related to steric hindrance of diffusion, whereas the C-term effect is related to the fact that the long straight channels (AR=4), resulting in less dispersion than short channels wherein the flow is continuously split and recombined [38]. The difference with the work of Sukas *et al* is that we introduce lateral elongation of the pillars (all the structures studied by Sukas were elongated in the axial direction). This lateral extension resulted in a drastic reduction of the B-term compared to the work described by Sukas. This will allow us to enter in a new separation regime wherein much higher plate counts can be theoretically achieved (see Fig. 8), i.e. passing the plate count limit observed for non-laterally extended pillars of N=2.5 10^5 to N=3.7 10^5. Note that we are using a 5 µm spacing (compared to the 2 µm spacing in Sukas). Scaling the laterally elongated channel to similar dimensions as used in Sukas would increase the plate height and hence the separation performance gain

further. The slight unfavorable decrease in electroosmotic mobility (K_v) for the rectangles (reduction from 6×10^{-9} m^2/Vs to 4×10^{-9} m^2/Vs) has a lower impact on the kinetic performance than the favorable plate height gain in H (also related to the fact that the kinetic performance scales with H^2/K_v).

Table 4: The analysis time and the produced number of plates at different points of kinetic plot representation for rectangular pillar structure. The applied voltage drop iss 20 kV.

N	1.0×10^5	2.5×10^5	4.5×10^5
***t* (min)**	2.4	27	296
***L* (m)**	0.11	0.36	1.19

A drawback of the non-porous pillars used here is that we have a too low phase ratio to conduct systematic retained experiments at this stage and that concentration overloading is significant and in fact too large to conduct retained measurements for relevant concentrations. In a next phase, we will incorporate porous silica glass by sol-gel methods that we recently developed for pressure-driven pillar-based LC. In a future study, we will incorporate recently developed porous glass deposition procedures to perform CEC separations under retained conditions.

Conclusions

Lateral extension of pillar shape (AR=4) yielded an increase in performance (in terms of plate height) compared to lower aspect ratio (AR=1) structures. As in pressure-driven LC, sidewall effects also play a significant role in CEC, roughly doubling the plate height. The attainable minimal plate height was 1.46 µm for unretained runs at the optimum working condition, compared to 1.90 µm for cylinders (in absence of sidewall effect). Due to steric obstruction of axial diffusion, the minimal plate height decreases when the aspect ratio of the pillars increases,

which is reflected in a reduced B-term at high AR. A kinetic plot analysis revealed that the high aspect ratio structures are key in in bringing attainable plate number values of CEC to larger values (current limit for AR<1 pillars), paving the way to obtaining N=500,000 plates.

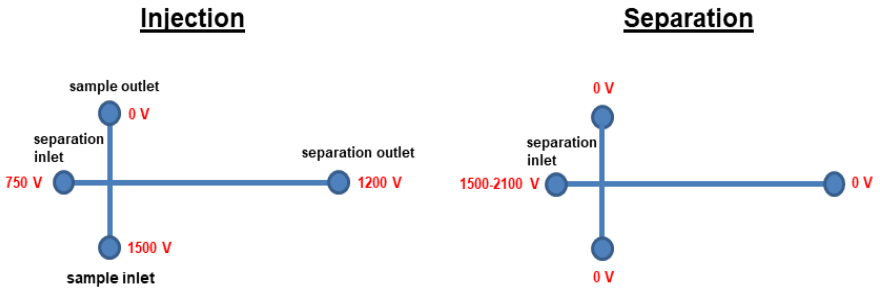

Fig. 1: Applied electric potentials at the reservoirs for injection and separation.

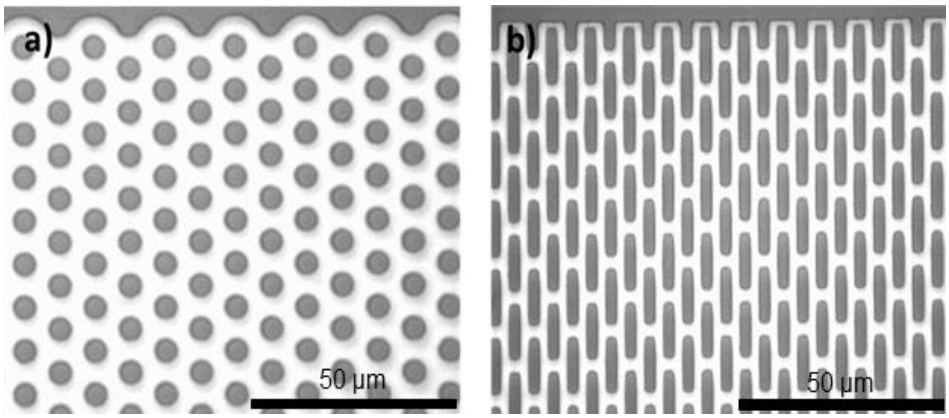

Fig. 2 Optical images of the structure designs employed during the study. A) Cylinders, B) Rectangles.

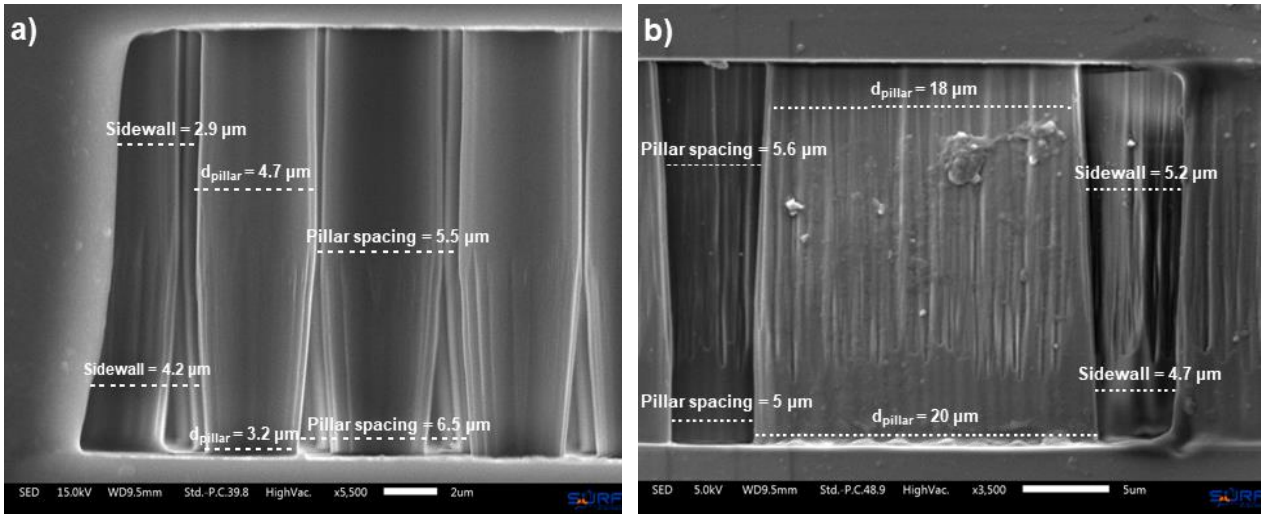

Fig. 3 SEM cross section pictures of column containing cylindrical pillars (a) and rectangles.

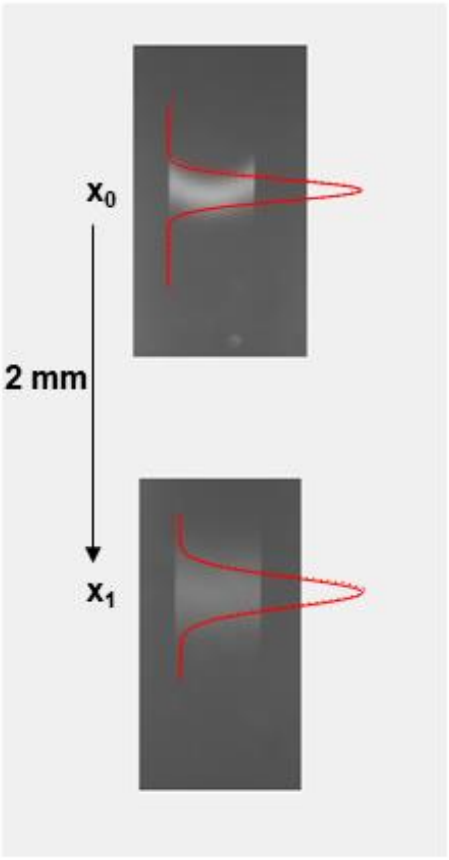

Fig. 4 Injected plug band profile at initial position (x_0) and final position (x_1) at a distance of 2 mm from x_0.

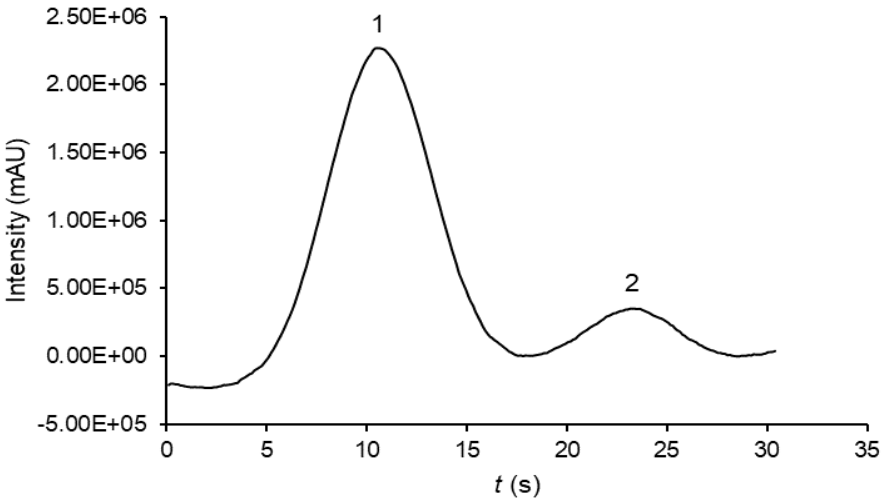

400

401 **Fig. 5** 2 coumarin dyes (C440, C480) separated at 300 V/cm (u_0 = 0.16 mm/s) with ODS-
402 modified cylindrical pillar array column using 50 mM phosphate buffer (pH 7) with 60:40
403 MeOH volumetric ratio as a mobile phase. Horizontal axis represents elapsed time after
404 injection. Retention factors: k_{C440} = 0, k_{C480} = 1.24.

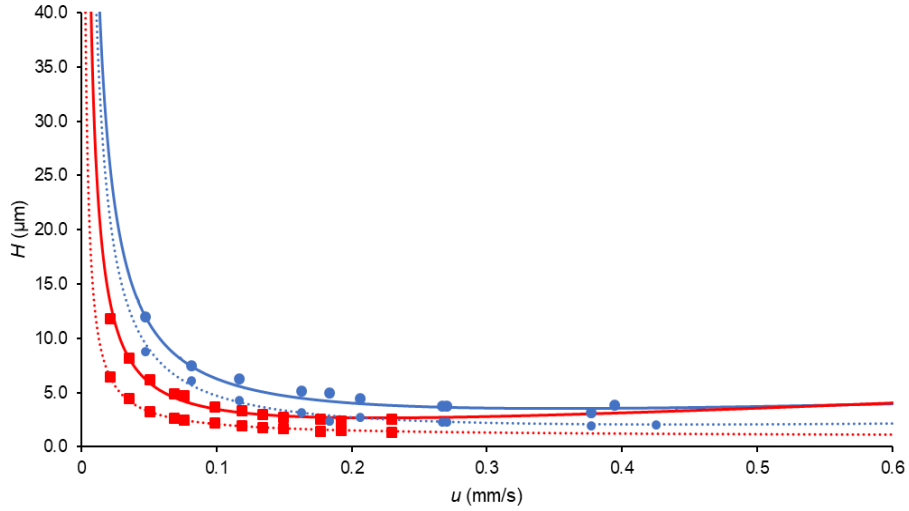

405

406 **Fig. 6** Van Deemter plots of the measured plate height against the mobile phase velocity under
407 non-retained conditions. Experimental results for different shapes: blue circles correspond to
408 the cylindrical pillar array column; red squares correspond to the rectangular pillar array
409 column. Full lines correspond to van Deemter including side walls, and dotted lines correspond

to van Deemter without side wall effect. Mobile phase: 50% methanol/buffer phosphate, pH 7 (v/v). measurement temperature: 25 °C, solute: 5 mM C440.

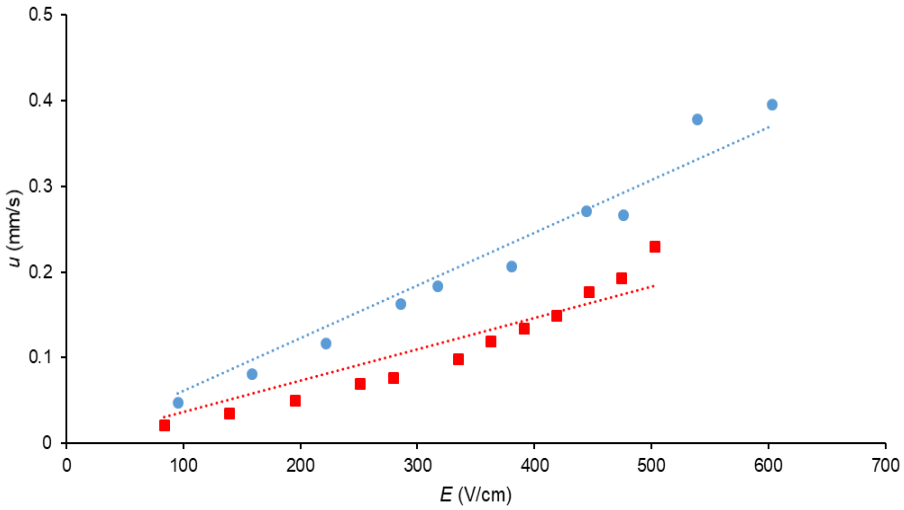

Fig. 7 Variation of the mobile phase velocity versus applied electric field strength. A linear curve fit intercepting at (0, 0) was implemented. The measured values of the electrokinetic permeability are 6.0×10^{-9} m^2/Vs for cylinders, 4.0×10^{-9} m^2/Vs for rectangles.

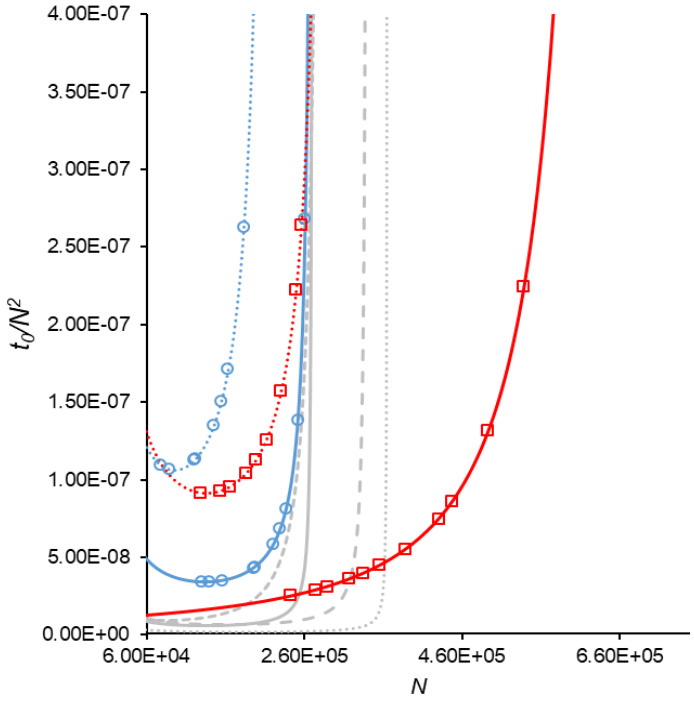

Fig. 8 Kinetic plot representation of the relationship between the analysis time and the produced number of plates. The blue line corresponds to cylindrical structures, whereas the red line corresponds to rectangular structures. The dotted blue line and the solid blue line correspond to column kinetic performance with sidewall effect and without sidewall effect, respectively. The dotted red line and the solid red line correspond to column kinetic performance with sidewall effect and without sidewall effect, respectively. Circles and squares represent the corresponding Van Deemter points. The round dot grey line corresponds to foil 0°. Square dot grey line corresponds to Foil 25°. Solid grey line corresponds to diamond and dashed grey line corresponds to hexagon. Values at optimal conditions: Cylindrical pillars (including sidewall effect): N_{opt} = 1.8×10^5, t_0 = 130 min, L = 96.8 cm; Rectangular structure (including sidewall effect): N_{opt} =2.4×10^5, t_0 = 177 min, L = 92 cm. Cylindrical pillars (not accounting for the side-wall effect): N_{opt} = 2.5×10^5, t_0 = 130 min, L = 96.8 cm; Rectangular structure (not accounting for the side-wall effect): N_{opt} =4.5×10^5, t_0 = 296 min, L = 1.19 m. The applied voltage drop iss 20 kV.

Acknowledgements

W.D.M. and M.B. greatly acknowledge the European Research Council for support through an ERC Starting Grant (number 679033EVODIS ERC-2015-STG).

References

[1] Colon, A. L., Burgos, G., Maloney, D. T., Citron, M. J., Rodriguez, R.L. Recent progress in capillary electrochromatography. *Electrophoresis* 2000, 21, 3965-3993.

[2] Vanhoenacker, G., Van den Bosch, T., Rozing, G., Sandra, Pat. Recent applications of capillary electrochromatography. *Electrophoresis* 2001, 22, 4064–4103.

[3] Dittmann, M.M., Rozing, G.P. Capillary electrochromatography–A high-efficiency micro-separation technique. *J. Chromatogr. A* 1996, 744, 63–74.

[4] Pretorius, V., Hopkins, B.J., Schieke, J.D. Electro-osmosis – New concept for High-Speed Liquid Chromatography. *J. Chromatogr.* 1974, 99, 23–30.

[5] Jorgenson, J.W., Lukacs, K.D. High-resolution separations based on electrophoresis and electroosmosis. *J. Chromatogr*., 1981, 218, 209-216.

[6] Knox, J.H., Grant, I.H. Miniaturisation in pressure and electroendosmotically driven liquid chromatography: Some theoretical considerations. *Chromatographia*, 1987, 24, 135

[7] Knox, J.H. Thermal effects and band spreading in capillary electro-separation. *Chromatographia* 1988, 26, 329-337.

[8] Knox, J.H., Grant, I.H. Electrochromatography in packed tubes using 1.5 to 50 μm silica gels and ODS bonded silica gels. *Chromatographia* 1991, 32, 317-328.

[9] C. Rice, R. Whitehead, J. *Phys. Chem*., 1965, 69, 4017.

[10] Rathore, A.S., Horvath, C. Capillary electrochromatography: theories on electroosmotic flow in porous media. *J. Chromatogr. A* 1997, 781, 185–195.

[11] Bartle, D. K., Myers, P. Theory of capillary electrochromatography, *J. Chromatogr. A* 2001, 916, 3–23.

[12] S. Rathore., A. Joule heating and determination of temperature in capillary electrophoresis and capillary electrochromatography columns, *J. Chromatogr. A* 2004, 1037, 431–443.

[13] Colon, L.A., Reynolds, K., Burgos, G., Moloney, T.D., Lopez, J. Studies of Submicron Particles and Electroosmotic Flow in Packed Capillary Columns for CEC. *Chromatography: J. Sep. and detect. Sci.*1999, 20, 306.

[14] R. Dadoo, R., Zare, R.N., Yan, C., Anex, D.S. Advances in capillary electrochromatography: rapid and high-efficiency separations of PAHs, *Anal. Chem.* 1998, 70, 4787–4792.

[15] Ludtke, S., Adam, T., Unger, K.K. Application of 0.5-mu m particles porous silanized silica beads in electochromatography, *J. Chromatogr. A* 1997, 786, 229–235.

[16] Smith, N.W., Evans, M.B. The analysis of pharmaceutical compounds using electrochromatography. *Chromatographia* 1994, 38, 649.

[17] Rapp, E., Bayer, E. Improved column preparation and performance in capillary electrochromatography, *J. Chromatogr. A* 2000, 887, 367–378.

[18] Ishizuka, N., Minakuchi, H., Nakanishi, K., Soga, N., Nagayama, H., Hosoya, K., Tanaka, N. Performance of a monolithic silica column in a capillary under pressure-driven and electrodriven conditions. *Anal. Chem.* 2000, 72, 1275–1280.

[19] Wen, E., Asiaie, R., Horvath, C. Dynamics of capillary electrochromatography II. Comparison of column efficiency parameters in microscale high-performance liquid chromatography and capillary electrochromatography. *J. Chromatogr.* 1999, A855, 349–366.

[20] Cikalo, M.G., Bartle, K.D., Myers, P. Influence of the electrical double-layer on electroosmotic flow in capillary Electrochromatography. *J. Chromatogr. A* 1999, 836, 35–51.

[21] Messina, A., Desiderio, C., De Rossi, A., Bachechi, F., Sinibaldi, M. Capillary electrochromatography on methacrylate based monolithic columns: evaluation of column performance and separation of polyphenols. *Chromatographia* 2005, 62, 409–416.

[22] Lynen, F., Buica, A., de Villiers, A., Crouch, A., Sandra, P. An efficient slurry packing procedure for the preparation of columns applicable in capillary electrochromatography and capillary electrochromatography-electrospray-mass spectrometry. *J. Sep. Sci.* 2005, 28, 1539–1549.

[23] Puangpila, C., Nhujak, T., El Rassi, Z. Investigation of neutral monolithic capillary columns with varying n-alkyl chain lengths in capillary Electrochromatography. *Electrophoresis* 2012, 33, 1431–1442.

[24] De Smet, S., Lynen, F. Kinetic performance evaluation and perspectives of contemporary packed column capillary electrochromatography. *J. Chromatogr. A*, 2014, 1355, 261–268.

[25] Henley Hampton, W., Jorgenson, W. J. Ultra-high voltage capillary electrophoresis >300 kV: Recent advances in instrumentation and analyte detection. *J. Chromatogr. A*, 2012, 1261, 171– 178.

[26] Masliyah, J.H., Bhattacharjee, S. Electrokinetic and Colloid Transport Phenomena. Wiley-Interscience, New Jersey, 2006.

[27] Jacobson, S.C., Hergenröder, R., Koutny, L.B., Ramsey, J.M. High-Speed Separations on a Microchip. *Anal. Chem.* 1994, 66, 7, 1114-1118.

[28] He, B., Tait, N., Regnier, F. Fabrication of Nanocolumns for Liquid Chromatography. *Anal. Chem*. 1998, 70, 3790−3797.

[29] Slentz, B. E., Penner, N. A., Regnier, F. Geometric effects of collocated monolithic support structures on separation performance in microfabricated systems. *J. Sep. Sci.* 2002, 25, 1011−1018.

[30] F. E. Regnier, Microfabricated Monolith Columns for Liquid Chromatography. Sculpting Supports for Liquid Chromatography. *J. High Resol. Chromatogr.*, 2000, 23, 19–26.

[31] Sukas, S., De Malsche, W., Desmet, G., Gardeniers H. J.G.E. Performance Evaluation of Different Design Alternatives for Microfabricated Nonporous Fused Silica Pillar Columns for Capillary Electrochromatography. *Anal. Chem.* 2012, 84, 9996−10004.

509 [32] Aoyama, C., Saeki, A., Noguchi, M., Shirasaki, Y., Shoji, S., Funatsu, T., Mizuno, J.,
510 Tsunoda, M. Use of folded micromachined pillar array column with low-dispersion turns for
511 pressure-driven liquid chromatography, *Anal. Chem.* 2010, 82, 1420–1426.

512 [33] Song, Y., Noguchi, M., Takatsuki, K., Sekiguchi, T., Mizuno, J., Funatsu, T., Shoji, S.;
513 Tsunoda, M. Integration of pillar array columns into a gradient elution system for pressure-
514 driven liquid chromatography, *Anal. Chem*. 2012, 84, 4739–4745.

515 [34] Taylor, L. C., Lavrik, N. V., Sepaniak, M. J. High-aspect-ratio, silicon oxide-enclosed
516 pillar structures in microfluidic liquid chromatography, *Anal. Chem.* 2010, 82, 9549–9556.

517 [35] Lavrik, N. V., Taylor, L. C., Sepaniak, M. J. Enclosed pillar arrays integrated on a fluidic
518 platform for on-chip separations and analysis, *Lab Chip* 2010, 10, 1086–1094.

519 [36] De Malsche, W., Eghbali, H., Clicq, D., Vangelooven, J., Gardeniers, H., Desmet, G.
520 Pressure-driven reverse-phase liquid chromatography separations in ordered nonporous pillar
521 array columns, *Anal. Chem.* 2007, 79, 915–5926.

522 [37] De Malsche, W., Op De Beeck, J., De Bruyne, S., Gardeniers, H., Desmet, G.; Realization
523 of 1×10^6 theoretical plates in liquid chromatography using very long pillar array columns,
524 *Anal. Chem.* 2012, 84, 1214–1219.

525 [38] Op De Beeck, J., Callewaert, M.; Ottevaere, H., Gardeniers, H., Desmet, G., De Malsche,
526 W. On the Advantages of Radially Elongated Structures in Microchip-Based Liquid
527 Chromatography. *Anal. Chem*. 2013, 85 (10), 5207-5212.

528 [39] Callewaert, M., Desmet, G., Ottevaere, H., De Malsche, W. Detailed kinetic performance
529 analysis of micromachined radially elongated pillar array columns for liquid chromatography.
530 *J. Chromatogr. A* 2016, 1433, 75–84.

[40] Jansen, H.V., de Boer, M.J., Unnikrishnan, S., Louwerse, M., C., Elwenspoek, M.C. Black silicon method, X: a review on high speed and selective plasma etching of silicon with profile control, *J. Micromech. Microeng.* 2009, 19, 033001.

[41] De Malsche, W., De Bruyne, S., Op De Beeck, J., Sandra, P., Gardeniers, H., Desmet, G., Lynen. Capillary LC separations using non-porous pillar array columns, *J. Chromatogr. A*, 2012, 1230, 41-47.

[42] Op De Beeck, J., De Malsche, W., Tezcan, S.T., De Moor, P., Van Hoof, C., Desmet, G. Impact of the limitations of state-of-the-art microfabrication processes on the performance of pillar array columns for LC, *J. Chromatogr. A*, 2012, 1239, 35-48.

[43] Op De Beeck, J., Callewaert, M., Ottevaere, H., Gardeniers, H., Desmet, W., De Malsche, W. Suppression of the side-wall effect in pillar array columns with radially elongated pillars, *J. Chromatogr. A*, 2014, 1367, 118-122.

[44] Desmet, G. Callewaert, M., Ottevaere, H., De Malsche, W., Merging open-tubular and packed bed liquid chromatography, *Anal. Chem.* 2015, 87, 7382–7388.

[45] Choudhary, G., Horvath, C. Dynamics of capillary electrochromatography. Experimental study on the electrosmotic flow and conductance in open and packed capillaries. *J. Chromatogr. A* 1997, 781, 161-183.

[46] Broeckhoven, K., Cabooter, D., Eeltink, S., Desmet, G. Kinetic plot-based comparison of the efficiency and peak capacity of high-performance liquid chromatography columns: Theoretical background and selected examples. *J. Chromatogr. A* 2012, 1228, 20-30.